X-Ray Diffraction Indicates That Active Cross-Bridges Bind to Actin Target Zones in Insect Flight Muscle

R. T. Tregear,* R. J. Edwards,# T. C. Irving,§ K. J. V. Poole,¶ M. C. Reedy,# H. Schmitz,‖ E. Towns-Andrews,** and M. K. Reedy#

*MRC Laboratory of Molecular Biology, Hills Road, Cambridge CB2 2QH, England; #Dept of Cell Biology, Duke University Medical Center, Durham, North Carolina 27710 USA; §Division of Biology, Illinois Institute of Technology, Chicago, Illinois 60616 USA: ¶Max-Planck-Institut für Medizinische Forschung, 6900 Heidelberg, Germany; ‖Institute of Molecular Biophysics, Florida State University, Tallahassee, Florida 32306-3015 USA; and **SERC Daresbury Laboratory, Daresbury, Warrington WA4 4AD, England

ABSTRACT We report the first time-resolved study of the two-dimensional x-ray diffraction pattern during active contraction in insect flight muscle (IFM). Activation of demembranated *Lethocerus* IFM was triggered by 1.5–2.5% step stretches (risetime 10 ms; held for 1.5 s) giving delayed active tension that peaked at 100–200 ms. Bundles of 8–12 fibers were stretch-activated on SRS synchrotron x-ray beamline 16.1, and time-resolved changes in diffraction were monitored with a SRS 2-D multiwire detector. As active tension rose, the 14.5- and 7.2-nm meridionals fell, the first row line dropped at the 38.7 nm layer line while gaining a new peak at 19.3 nm, and three outer peaks on the 38.7-nm layer line rose. The first row line changes suggest restricted binding of active myosin heads to the helically preferred region in each actin target zone, where, in rigor, two-headed lead bridges bind, midway between troponin bulges that repeat every 38.7 nm. Halving this troponin repeat by binding of single active heads explains the intensity rise at 19.3 nm being coupled to a loss at 38.7 nm. The meridional changes signal movement of at least 30% of all myosin heads away from their axially ordered positions on the myosin helix. The 38.7- and 19.3-nm layer line changes signal stereoselective attachment of 7–23% of the myosin heads to the actin helix, although with too little ordering at 6-nm resolution to affect the 5.9-nm actin layer line. We conclude that stretch-activated tension of IFM is produced by cross-bridges that bind to rigor's lead-bridge target zones, comprising $\leq$1/3 of the 75–80% that attach in rigor.

INTRODUCTION

Myosin motors are postulated to produce force and filament sliding by changing angle while attached to actin (Huxley, 1969; Rayment et al., 1993). This "cross-bridge" hypothesis has stimulated efforts to monitor the structure and action of working cross-bridges by numerous biophysical methods to identify structural changes that mark the transition from rest to contraction. X-ray diffraction can be used to observe the pattern of actomyosin attachment during muscle contraction. In vertebrate skeletal muscle, activation produces a small rise in intensity in the unsampled medium- and low-angle layer lines based on actin, consistent with either the labeling of a small fraction of actin sites by stereospecifically bound myosin heads, or with the decoration of a larger actin fraction by a sterically diverse range of myosin head shapes and binding interfaces (Huxley and Kress, 1985; Yagi, 1991; Wakabayashi et al., 1991; Harford and Squire, 1992; Bordas et al., 1993; Bershitsky et al., 1997). Electron microscope images from quick-frozen active vertebrate skeletal muscles have shown both a rise in actin-based ordering of cross-bridges (Tsukita and Yano, 1985; Hirose et al., 1993; Lenart et al., 1996) and preferred shapes for attached cross-bridges (Hirose et al., 1994), whereas the equatorial x-ray diffraction from active muscle has been interpreted in terms of a force-generating cross-bridge form different from those seen in rigor or relaxed muscle (Brenner and Yu, 1993). However, the number, structures, and pattern of attachment for active cross-bridges remain to be established.

Insect flight muscle (IFM) from *Lethocerus* is well suited to the study of working cross-bridges, in part because it can be stretch activated. In vivo, nerve stimulation serves to prime the contractile apparatus by raising the cytosolic calcium concentration; full activation is achieved only after a small stretch. In vitro, tension generation can be experimentally separated from calcium binding (Jewell and Ruegg, 1966). Demembranated IFM fibers, after being equilibrated in a "priming" calcium concentration, allow active tension generation to be subsequently triggered by a stretch. This allows all sarcomeres in a bundle of skinned fibers to be activated simultaneously and repetitively, an experimental amenity not available in skinned vertebrate striated muscle. Demembranated IFM can also be activated by a higher calcium concentration without stretching, but the present study is confined to stretch activation.

A considerable amount is already known of the structure of the *Lethocerus* IFM cross-bridge because of its unexcelled paracrystalline order, and because the interacting thick and thin filaments are coplanar, so that cross-bridges are fully visible in thin section without interference from out-of-plane cross-bridges (Reedy et al., 1965; Reedy and Reedy, 1985; Taylor et al., 1989a,b). The myosin heads of

Received for publication 11 March 1997 and in final form 25 November 1997.

Address reprint requests to Dr. Richard Tregear, Structural Studies Division, MRC Laboratory of Molecular Biology, Hills Road, Cambridge CB2 2QH, England. Tel.: 44-1223-365963; Fax: 44-1223-213556; E-mail: rt1@mrc-lmb.cam.ac.uk.

0006-3495/98/03/1439/13 $2.00

ATP-relaxed IFM ("detached cross-bridges") are arranged in 14.5-nm-spaced shelves projecting at 90° from the thick filaments (Menetret et al., 1990; Reedy et al., 1992), in contrast to the axially splayed myosin heads of vertebrate striated muscle thick filaments (Harford and Squire, 1986; Levine, 1993; Irving, 1993). In rigor IFM, cross-bridges bind to actin in doublet pairs at each half-turn of the 39-nm actin helix, the sterically favored "target zone" (Reedy, 1968), showing that rigor cross-bridge binding occurs at a particular azimuthal presentation of actin sites to thick filaments. Weakening the rigor bond by binding AMPPNP (adenylylimidodiphosphate) to the myosin leaves the most sterically favored of the IFM cross-bridges still attached to the same "lead bridge" target zone (Reedy et al., 1987, 1988; Winkler et al., 1996; Schmitz et al., 1996). Target zone binding has also been recognized in rigor vertebrate muscle, despite the less favorable geometry of the vertebrate lattice (Varriano-Marston et al., 1984; Squire and Harford, 1988). Although it has been proposed from time to time that active cross-bridges may, like rigor bridges, bind preferentially to target zones (e.g., Lenart et al., 1996), there has until now been no direct evidence to show that this is so.

Previous x-ray diffraction studies of stretch-activated IFM were restricted to the strong reflections on the equator and meridian of the diagram, owing to the brevity of the event and the weakness of other reflections (Armitage et al., 1975; Rapp et al., 1991). Our work here is the first to report a time-slicing study of the full two-dimensional x-ray diagram from IFM during activation. To learn if the attachment of active, force-generating cross-bridges might be restricted to azimuthally favored target zones, it is necessary to examine the lattice-sampled inner layer lines, whose intensities are dependent on actin-based order. The newly available high-flux low-angle beam line and high-efficiency two-dimensional counter at the SRS synchrotron allowed us to record the intensities of these inner layer line peaks during stretch activation and to relate the time course of layer line intensity changes to that of active tension.

METHODS

Longitudinal flight muscle was ventrally and medially exposed in opened hemithoraces of the tropical Belostomatid waterbug *Lethocerus indicus*, then glycerol extracted in situ as described (Reedy and Reedy, 1985), by slow tumbling in pH 6.8 relaxing buffer supplemented at first by detergent + antiprotease cocktail, then by 50% and 75% glycerol, and containing (in mM) 5 $MgCl_2$, 5 ATP, 5 EGTA, 5 NaN_3, 100 KCl, and 20 KPO_4 buffer. Muscles were stored at −105°C in cryovitrified 75% glycerol relaxing buffer, with 5 mM dithiothreitol added, for up to 1 year, then kept just before use for 8–15 days at −80°C and for 0.5–3 h at −20°C. The 16 mm × 70 μm fibers were dissected out and used as required. Bundles of 8–12 fibers were mounted with cellulose nitrate cement to longitudinally aligned stainless steel rods on a muscle mechanical setup (Güth Muscle Research System; Scientific Instruments for Muscle Research, Heidelberg; cf. Güth and Wojciechowski, 1986) in a relaxing solution containing no added KCl or phosphate (11 $MgCl_2$, 10 ATP, 5 EGTA, 20 3-(*N*-morpholino)-2-hydroxypropanesulfonic acid, 5 NaN_3, pH 6.8, ionic strength 0.10), between windows of either Mylar or (more usually) thin mica and oriented in the path of 1.4-Å x-rays from a synchrotron source (Station 16.1; S.R.S., Daresbury, England), focused on a 2D wire detector 2.8 m behind the specimen. Once satisfactory mechanics and diffraction were obtained, the solution was changed to one of a priming calcium concentration sufficient to make the fibers stretch activate, but which did not greatly raise the tension in the unstretched muscle (components and pH as for the relaxing solution plus 3.75 mM $CaCl_2$; the free calcium, calculated from the stability constants of the ionic complexes, was 3 μM). The active tension response to stretch was maximized by adjustment of the static extension (0.2–1.0% of L_0) and the amplitude of stretch (1.5–2.5% of L_0); a slowed square wave (time constant 10 ms) was used to generate the step stretch, to minimize mechanical damage due to repeated stretches. The muscle fiber bundle was then submitted to a routine of 10 1.5-s stretches spaced at 30-s intervals, during which time-sliced x-ray exposures were made before and during each stretch (Fig. 1 *A*). Diffraction data were collected as 50- or 1000-ms time frames (Fig. 1 *A*) and stored for off-line analysis. Similar experiments were also performed in relaxing solution, and occasional rigor exposures were taken in rigor (solution = relaxing solution without MgATP).

Experiments were selected for analysis on the basis of satisfactory mechanics and diffraction; six active-stretch and four relaxed-stretch runs were used. The diffraction data were analyzed with the SRS fiber diffraction analysis packages BSL and XOTOKO (courtesy of G. R. Mant). By using BSL, all recorded patterns were initially corrected, first by subtracting a properly scaled detector response blank exposed during the same 24-h shift. Then the four quadrants were reassembled to the nearest pixel to eliminate the empy central "TAC cross-" detector feature, then rotated to

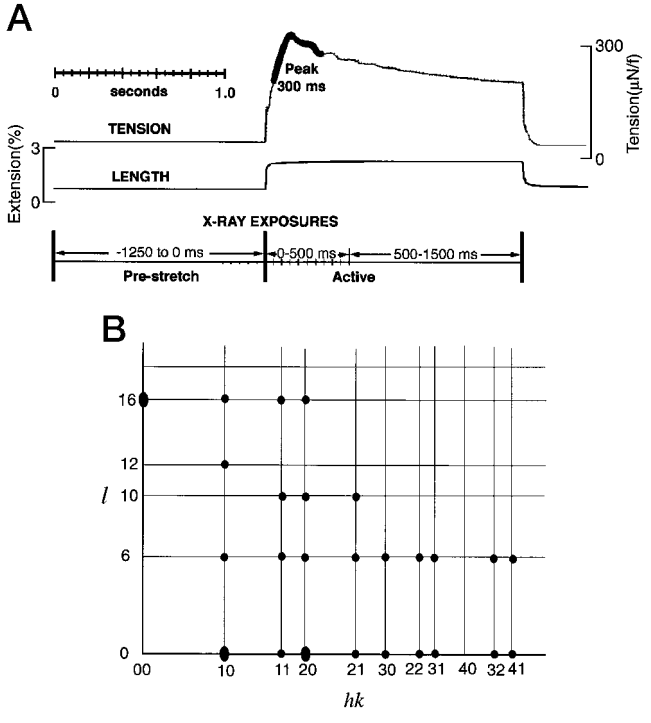

FIGURE 1 (*A*) Schematic of the data collection. Diffraction was collected from a 2D detector as a series of time frames: 1 × 1 s, followed by 5 × 50 ms before stretch, 10 × 50 ms and 1 × 1 s after stretch. For each experiment this protocol was repeated 10 times at 30-s intervals, and the data were summed. The fibers were slightly stretched during each interval, so as to maintain the small steady tension needed to allow the sudden stretch to cause a large delayed tension. The vertical scale for tension starts from zero, and that for extension from slack length. (*B*) Schematic of the *Lethocerus* flight muscle diffraction diagram. Lattice indices (hk.l) are based on a unit cell of 232-nm axial repeat. The low-angle layer lines observed were the equator (l = 0), the 38.7 nm (l = 6), 23 nm (l = 10), 19.3 nm (l = 12), 14.5 nm (l = 16), and 12.9 nm (l = 18). The principal peaks observed are marked on the intersections of row and layer lines.

make the meridian exactly vertical, and centered in the 512 × 512 pixel image frame. All patterns were then symmetrized by quadrant folding about the center and added together to sum both serial time frames within experiments and corresponding time frames from parallel experiments.

The pattern was indexed as hk.l reflections on the filament lattice (a, b = 52 nm) and on the long repeat, in which both myosin and actin periods can be expressed (c = 232 nm; Fig. 1 *B*). Equatorial slices of each record were made to isolate the equator: the 38.7 nm, 19.3 nm, and 14.5 nm layer lines (the 6th, 12th, and 16th layer lines as indexed on 232 nm; Fig. 1 *B*). The slice width was set to include ~40% of the interlayerline spacing. XOTOKO was then applied to these layer line slices to make and measure graphic intensity profiles along each slice, to extract the lattice-sampled peak counts and the background between them. First the lattice spacing and the full width half-maximum (FWHM) equatorial width of the peaks were extracted from the equatorial data. The position of the row lines was thus determined (see Fig. 1 *B* for indexing of peaks). The background was determined from lowest-count positions midway between row lines (more than two times the FWHM from the center of any peak) and calculated for the row lines. Counts were collected from a fixed number of channels about the row-line centers, and the background was subtracted. In the case of the closely overlapping 22.6 and 31.6 intensities, the centers were found to be separated by ~1.2 times the FWHM of each peak; accordingly, the contribution of each reflection to the merged peak was estimated by collecting the counts in the channels between the peaks and subtracting from this the counts in the same number of channels outside the other one of the paired peaks. The 00.16, 00.32, and 20.0 intensities are cited as their entire two-quadrant value (i.e., from both sides of the equator or meridian), in accordance with our previous practice (Holmes et al., 1980; Tregear et al., 1990), and so are doubled with respect to the one-quadrant values for other reflections. Within a given pattern, intensities are expressed relative to that of the 20.0 equatorial reflection. Changes in the 20.0 reflection intensity under varying conditions are cited relative to its value in relaxation. In two of the six experiments, the change to calcium-priming solution caused a considerable loss in the 20.0 equatorial intensity. This was probably due to specimen movement in the x-ray beam, as the equatorial background also fell, and as previous observations have shown the usual response to be a small increase in the 20.0 reflection with the addition of calcium (Armitage et al., 1975; Rapp et al., 1991). Because of these variations, the effect of stretch activation on the 20.0 was assessed from the other four experiments. The data on all of the other reflections were normalized in each experiment individually relative to the 20.0 equatorial obtained under the same experimental conditions (relaxation, prestretch, stretched, or rigor).

Patterns were prepared for display (Fig. 2) using BSL. Each pattern was symmetrized by four-quadrant folding about the center and normalized to make it equivalent to the longest summed exposure of 50 s. It was then adjusted (by setting "threshold levels" in BSL's DISPLAY command) to create a set of four output images, representing four different relative "exposures." A Macintosh X-Window emulator (Xoftware 3.0, from Age Logic, San Diego, CA) was used to cut and paste these four versions from BSL's UNIX home platform on a Silicon Graphics workstation into Adobe Photoshop (Adobe Software) files on a Macintosh PowerPC 7100 computer. The images in Fig. 2 were composed in Photoshop by overlaying and aligning the central parts of successively lighter "exposures" to show detail hidden in the "overexposed" central region of the underlying next darkest "exposure." No adjustment of image density or contrast was performed in Photoshop.

RESULTS

In the absence of calcium, ATP-relaxed IFM fibers stretched slightly over their slack length held a tension of ~20 μN/fiber and produced no delayed tension on dynamic stretch. When the free calcium concentration was raised to 3 μM and the fibers were stretched slightly more, the fibers held a tension, on average, of 50 μN/fiber; we have termed this condition the calcium-primed state. When calcium-primed fibers were dynamically stretched by an optimal amplitude (range 1.3–2.4%), they generated delayed tension (Fig. 1 *A*), which peaked at, on average, 270 μN/fiber (additional tension of 210–340 μN/fiber, reached after a 110–170-ms delay). The active tension gradually decayed from this peak during a 1.5-s stretch (Fig. 1 *A*). Both the height of the tension peak and its decay have been shown to be a characteristic of the absence of phosphate (White and Thorson, 1972), but are not caused by ATP starvation, as they persist in the presence of a back-up system for ATP regeneration (White et al., 1977). At a calcium level greater than that necessary for priming, the fibers generated more steady tension before stretching, and showed less tension increase after stretch; in separate control experiments maximally calcium-activated fibers gave an average isometric tension of 440 μN/fiber (range 250–520 μN/fiber).

Relaxed IFM shows a highly ordered x-ray diffraction pattern, in which the inner layer lines are lattice-sampled and the outer ones are not (Fig. 2 *A*; Miller and Tregear, 1972). The layer lines can all be indexed on a 232-nm axial repeat (Fig. 1 *B*). Some layer lines arise from the thick filament order (l = 10, 16, 26, 32, 48, corresponding to axial spacings of 23.2, 14.5, 8.92, 7.25, 4.8 nm), others from the thin filaments (l = 12, 18, 39, corresponding to axial spacings of 19.3, 12.9, 5.95 nm), whereas the innermost layer line (l = 6; 38.7 nm) is mixed, coming from both four-start 155-nm helices on thick filaments and two-start 77-nm helices on thin filaments. In the present study we have concentrated on changes in the intensities of reflections on the 38.7, 19.3, 14.5, and 7.2-nm layer lines (l = 6, 12, 16 and 32). The 12.9-nm meridional reflection (l = 18) was not studied, because of its overlap with the strong 14.5-nm meridional reflection (Fig. 2, *A–D*).

Consistent changes in diffraction can be seen in the summated patterns from the experimental series (Fig. 2). Calcium-primed, unstretched fibers gave a diffraction pattern qualitatively similar to that in relaxing solution (Fig. 2, *A* and *B*). The principal changes that could be seen on calcium priming were that the 23.2-nm layer line weakened until it was barely visible and that both the 14.5-nm and 7.2-nm meridional reflections (00.16, 00.32) broadened toward the first row line. During the peak of tension generation after stretch, the calcium-primed fibers showed further striking changes in the diffraction pattern (Fig. 2, *B* and *C*; details shown in Fig. 2, *F* and *G*). Both the 00.16 and 00.32 reflections lost intensity and broadened further. The first row line peak on the 19.3-nm layer line (10.12) grew, becoming clearly visible, whereas the first row line peak on the 38.7-nm layer line (10.6) reflection dropped. Farther out on the 38.7-nm layer line, the 11.6, 21.6, and 31.6 reflections rose, whereas the 30.6 almost vanished. The smooth 5.9-nm layer line showed no obvious change. The diffraction remained similar throughout the applied stretch (Fig. 2 *D*). The changes seen were much smaller than the rigor changes found on removal of ATP (Fig. 2 *E*). Consistent with previous descriptions (Miller and Tregear, 1972;

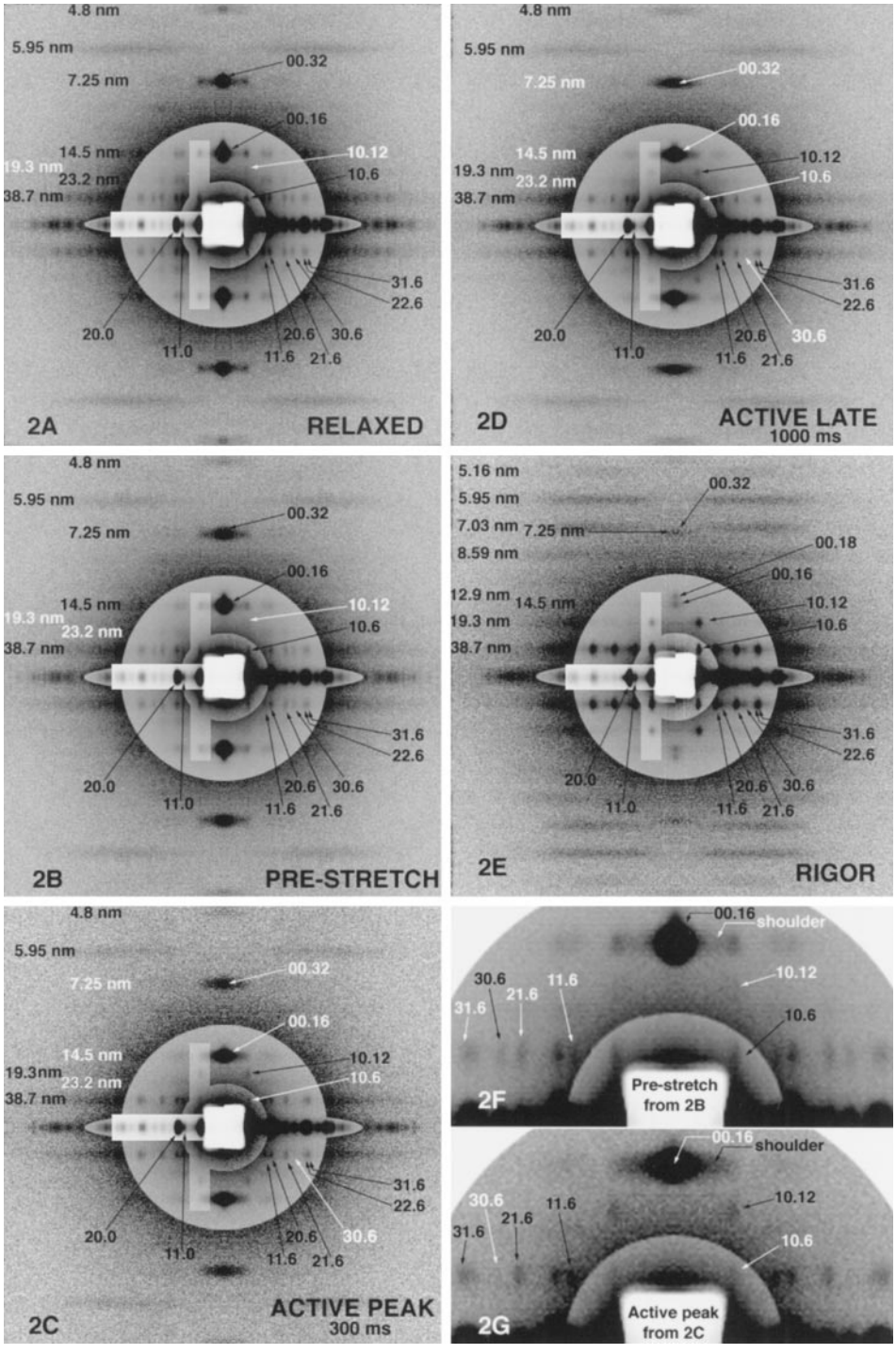

FIGURE 2 Diffraction patterns from insect flight muscle (IFM) of *Lethocerus* (*A*) in relaxation (<0.1 μM free calcium); (*B*) before stretch-activation in ~3 μM free calcium, a priming calcium concentration sufficient to support tension generation when a sudden stretch is applied, but which produced little tension in unstretched fibers; (*C*) 50–350 ms after the application of such a stretch; (*D*) 500-1500 ms after stretch; (*E*) in rigor, i.e., in the absence of ATP. *F* and *G* are enlarged from *B* and *C* to improve the visibility of main reflections discussed in the text. Patterns *A–D* are integrated from five fiber bundles of the stretch-activation protocol; pattern *E* is a typical rigor pattern from one fiber bundle. Total exposure times were 15 s (*C*), 20 s (*E*), and 50 s (*A*, *B*, *D*, *F*, *G*). Patterns were quadrant-folded and adjusted in BSL so as to equalize the exposure levels (to 50-s equivalent) throughout the set, then adjusted to derive three lighter "exposures" (*central regions*) in each case. The region of third lightest exposure (*central circle*) is extended in a vertical bar in *A–E* to compare 10.6 and 10.12 reflections within a single exposure level. Reflections that show intensity changes upon activation have gains indicated where white labels (in *A*, *B*, *F*) change to black (in *C*, *D*, *G*), and losses are indicated where black labels (in *A*, *B*, *F*) change to white (in *C*, *D*, *G*). In upper left quadrants, the leftmost column gives spacings of actin layer lines (38.7–51.6 nm), and the inner column gives spacings of myosin layer lines (23.2–4.8 nm), except for 38.7 nm, which is of mixed actin and myosin origin.

Holmes et al., 1980), we found that in rigor IFM the 00.16 and 00.32 reflections became very weak, whereas the 10.6, 10.12, 11.6, 21.6, and 31.6 reflections all became much stronger than in the activated pattern; the 5.9-nm layer line intensified toward the meridian; and a family of similarly unsampled outer layer lines appeared, forming a stack within which the 5.9-nm line was the strongest feature.

The effect of stretch activation was evaluated quantitatively in each of the six experiments performed. The background was subtracted from each reflection, and its intensity was expressed as a percentage of the 20.0 reflection intensity. The intensity of the IFM 20.0 reflection is known to rise by only a few percent during stretch activation (Rapp et al., 1991; see also last entry in Table 1 and Fig. 3 *N*). Analysis of individual experiments confirmed the deductions made from the summed diffraction patterns. Stretch activation halved the 00.16 intensity and reduced the 00.32 intensity by one-third (Table 1, last column). The 10.12 intensity tripled and the 10.6 intensity halved. The 11.6, 21.6, and 31.6 intensities each rose by around half, and the

TABLE 1 Intensities of lattice-sampled reflections in a calcium-priming solution before and during stretch activation

	Intensity (% $I_{[20.0]}$)		Change on stretch activation	
Reflection	[a] before stretch	[b] at tension peak	[c] as % $I_{[20.0]}$	[d] as fraction of [a]
00.16[#]	50.9 ± 9.0	23.2 ± 1.8	−27.69 ± 7.31*	−0.54
00.16_{sh}[#]	2.86 ± 0.25	4.26 ± 0.10	1.405 ± 0.290*	0.49
00.32	3.05 ± 0.31	2.19 ± 0.08	−0.87 ± 0.28*	−0.29
10.12	0.11 ± 0.03	0.34 ± 0.05	0.223 ± 0.048*	2.03
10.6	1.31 ± 0.10	0.70 ± 0.08	−0.616 ± 0.102*	−0.47
11.6	0.25 ± 0.04	0.37 ± 0.06	0.119 ± 0.028*	0.48
20.6	0.42 ± 0.02	0.50 ± 0.08	0.075 ± 0.066	0.18
21.6	0.27 ± 0.04	0.38 ± 0.05	0.112 ± 0.052	0.42
30.6	0.18 ± 0.03	0.01 ± 0.04	−0.167 ± 0.035*	−0.93
22.6	0.23 ± 0.04	0.18 ± 0.04	−0.049 ± 0.032	−0.21
31.6	0.25 ± 0.05	0.40 ± 0.05	0.147 ± 0.043*	0.59
20.0	101.4 ± 1.9	104.4 ± 2.8	2.96 ± 1.36	0.03

These are the responses to a stretch activation that generated a net active tension of 230 ± 16 μN/fiber above the calcium-primed prestretch baseline of 48 ± 15 μN/fiber. Intensities (except the 20.0) are cited relative to the 20.0 intensity under the same conditions. The 20.0 itself is cited relative to its value in relaxation. In each experiment the first six frames of diffraction were summed to obtain column [a] , frame 7 omitted, and frames 8–13 summed for column [b] (cf. Fig 1 *A*). Column [c] is derived from the change for each experiment. This change is also shown in column [d] as the fractional change from the initial value. Values shown are mean and SEM from $n = 6$ experiments (except for 10.12 ($n = 5$) and 20.0 ($n = 4$)).

*Significance was assessed by Student's *t*-test for n-2 d.f.; 5% level shown by asterisk.

[#]The 00.16 reflection was collected over an equatorial range from -0.01 nm^{-1} to $+0.01$ nm^{-1}. Its shoulder, 00.16_{sh}, was collected from 0.011 to 0.02 nm^{-1}.

30.6 fell nearly to zero. The results were consistent between experiments so that, with the exception of the 21.6, the average changes in these reflections were significantly different from zero (Table 1, column 4, *).

The time course of each of these changes was assessed at 100-ms time resolution (Fig. 3, *continuous lines*). The 00.16 reflection fell to a minimum intensity at the same time as the active tension peak and well after the length change (Fig. 3, *A–C*); the radial spread caused a rise in the 00.16 shoulder, which mirrored this time course (Fig. 3 *D*). The 00.32 reflection fell with a similar time course (Fig. 3 *E*). The 10.12 reflection rose to a peak at the same time as tension and then fell back sharply (Fig. 3 *F*); the fall and subsequent rise of the 10.6 reflection mirrored the 10.12 time course (Fig. 3 *G*). For the weaker reflections (Fig. 3, *H–M*), 100 ms was the highest resolution at which a time course could be discerned. Even at this low time resolution, occasional large deviations from the apparent time course occurred. These were sufficiently rare to have occurred by chance and were therefore not considered significant; only two of the 30 points in Figs 3, *H–M* (one in Fig. 3 *J*, one in in Fig. 3 *M*) clearly deviated by more than 0.15% (twice the estimated SD of the 100-ms points derived from the interexperimental variation; cf. legend to Fig. 3) from the trend of the other points. The trends in each of the 11.6, 21.6, and 31.6 reflections were unidirectional (Fig. 3, *H*, *J*, *M*), but the points were too scattered to infer a time course.

The meridional and first row-line reflections were further examined at 50-ms resolution (Fig. 4). Each intensity change was normalized, and its time course was compared to that of the stretch-induced tension. The 00.16 reflection could be seen to reach a minimum close to the tension peak and then to rise again more slowly than the tension fell; both the radial spread of the 00.16 reflection and the fall in the 00.32 followed a similar course (Fig. 4 *A*). The changes in the 10.12 and 10.6 reflections peaked within 50 ms of the tension peak (Fig. 4 *B*) and then returned faster than tension toward their prestretch values.

When the fibers were stretched by the same amount in calcium-free ATP-relaxing solution, there was no active tension, but the high stiffness of the muscle produced a large passive tension component (Jewell and Ruegg, 1966; Fig. 3 *B*, *dashed line*). There was little change in the diffraction pattern on stretch of relaxed IFM. The 23-nm layer line remained present (diffraction pattern not shown), and the 00.16 and 00.32 meridionals only fell by relatively small amounts, without obvious delay or appreciable lateral spread (Fig. 3 *C–E*, *dashed lines*). The changes in the weaker reflections were more scattered than those from stretch activation, probably because of the smaller number of experiments ($n = 4$), so that no time courses could be obtained. However, it could be seen that the effects of relaxed stretch on the first row line reflections, 10.6 and 10.12, were small, and much less than the changes in stretch activation (Fig. 3, *F* and *G*, *dashed lines*). The 11.6 and 21.6 fell, in contrast to the rise seen in stretch activation (Fig. 3, *H* and *J*, *dashed lines*). On the other hand, the 30.6 and 22.6 reflections both fell as much under passive extension as in activation (Fig. 3, *K* and *L*, *dashed lines*), whereas the 31.6 showed a small increase (Fig. 3 *M*, *dashed lines*).

DISCUSSION

Electron microscope and x-ray diffraction studies of IFM in rigor and AMPPNP states (Reedy and Reedy, 1985; Reedy

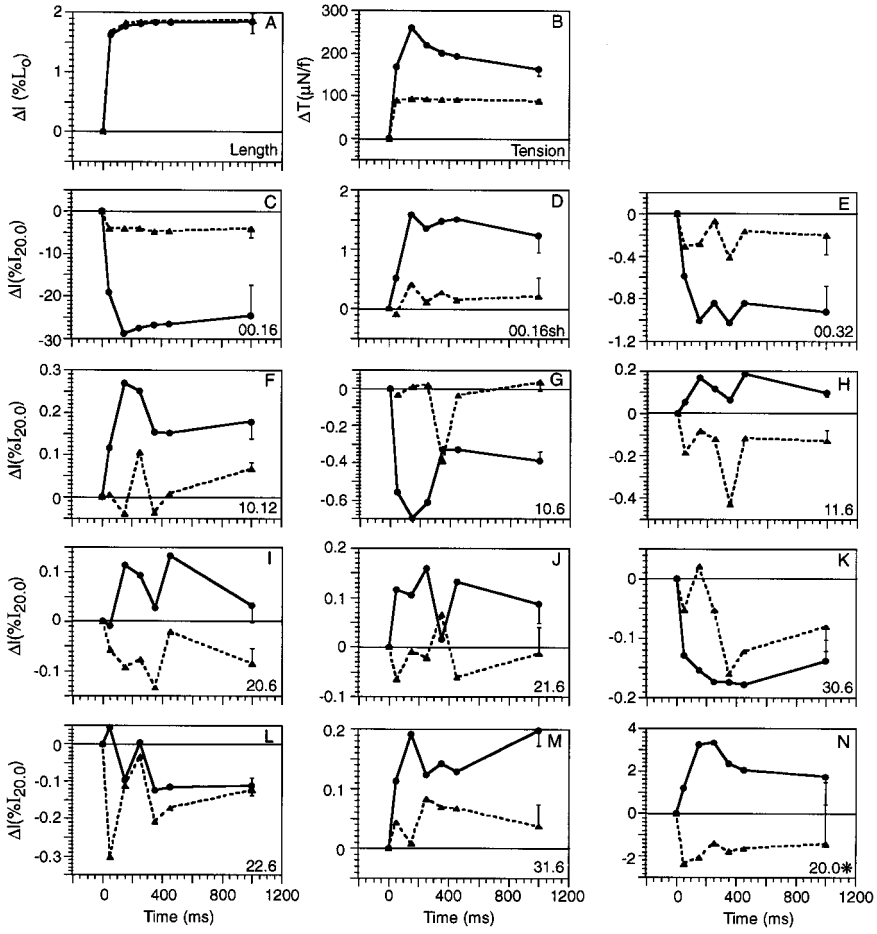

FIGURE 3 Time course of the change in (*A*) length (% initial length), (*B*) tension (μN/fiber), and (*C–N*) the changes in intensity of the lattice-sampled reflections when the muscle fibers were stretched in either activating solution (——) or relaxing solution (– – –). All intensities except the 20.0 reflection were normalized against the average value of the 20.0 reflection intensity during prestretch (for the first point) or stretch (for all subsequent points). The 20.0 reflection itself (Fig. 2 *N*) was normalized against its average value in relaxation and before stretch. Each point represents a 100-ms time frame. The zero point in each graph is taken from the mean value of the parameter during the 1.25 s before stretch, and the last point is taken from the value during the terminal 1 s of stretch (cf. Fig. 1). The error bars on the last points are SD values estimated from the SEM of the variation of the 1000-ms time frame values between the six experiments. The estimated SD of the 100-ms points was 0.076%, averaged over all of the data from the low-intensity reflections.

et al., 1987, 1988, 1993; Taylor et al., 1989a,b, 1993; Tregear et al., 1990; Schmitz et al., 1996, 1997; Winkler et al., 1996) have shown the structure of the myosin heads bound to actin in these near-static conditions. We are now trying to observe the cross-bridge structure under dynamic conditions, both in x-ray diffraction and in electron micrographs of quick-frozen active IFM. The aim of the present x-ray diffraction study was to see what changes occur in both actin-based and myosin-based reflections from IFM when the muscle is stretched to produce active tension. Until now, most of these reflections have proved too weak to be observed within the time scale allowed by the x-ray beams and detectors available. The new low-angle beamline and two-dimensional detector at SRS have made the current experiments possible. Previous x-ray diffraction studies of stretch-activated IFM, which were limited to the strongest near-meridional and equatorial reflections (Armitage et al., 1975; Rapp et al., 1991), found that the strong 14.5-nm meridional decreased, consistent with the movement of the relaxed heads away from the relaxed thick filament array, but did not find the increase in the 39-nm layer line and 20.0 equatorial reflections that might be expected on the attachment of myosin heads to actin.

In the full two-dimensional diffraction patterns reported here, we find changes in the 14.5-nm, 19-nm, and 39-nm reflection intensities that indicate displacement of some myosin heads from the relaxed array during stretch activation and actin attachment for a portion of these heads. As we discuss below, the rise in the intensities of several of the outer reflections on the 39-nm (6th) layer line indicates cross-bridge attachment, and the reciprocal rise and fall of the first row-line reflections on the 19-nm (10.12) and 39-nm (10.6) as tension develops suggest cross-bridge attachment to a specific, helically selective region of the actin filament, midway between the portions of the troponin complex that form a discrete lump every 39 nm along the actin filament.

The reciprocal intensity changes on the first row line

The reciprocal intensity changes in the first row-line reflections on the 19-nm and 39-nm layer lines are statistically significant, correlate temporally with active tension, and are absent when muscle fibres are similarly stretched in the absence of calcium. Their interpretation requires assignment of their structural origin, which we derive from a consideration of the rigor structure. In rigor IFM, lead and rear myosin cross-bridges attach every 39 nm. In each lead

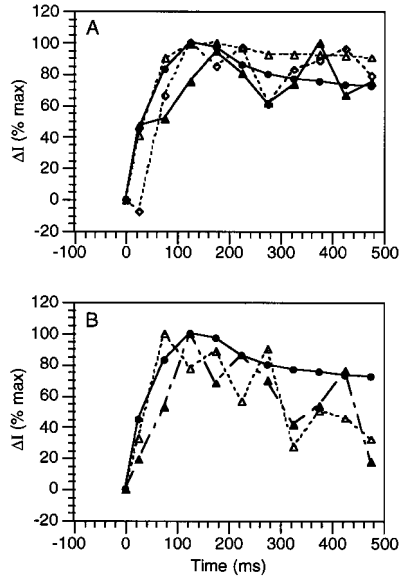

FIGURE 4 Time course of the normalized changes in (*A*) active tension (●), 00.16 reflection (△), 00.32 reflection (▲), and radial spread of 00.16 (◇); (*B*) active tension (●), 10.6 (△), and 10.12 reflections (▲). Time frames of 50 ms are plotted. These shorter time frames contain fewer counts and thus show less statistical smoothing than do the 100-ms frames of Fig. 3.

cross-bridge, two heads of one myosin molecule (Taylor et al., 1989a,b, 1993) bind along the actin helix at a particular region halfway between 39-nm-spaced bulges that have been identified by immunolabeling as part of the troponin complex (Reedy et al., 1994). Each rear cross-bridge contains one head of another myosin that binds close to the troponin (Reedy et al., 1987; Taylor et al., 1993; Winkler et al., 1996; Schmitz et al., 1996). Because the 39-nm actin helix repeat in IFM (Miller and Tregear, 1972) is the same length as both the rigor bridge repeat and the troponin bulge repeat found in electron micrographs (Taylor et al., 1989b, 1993), it follows that bridge attachment and troponin are each located at a distinct helical actin registration relative to the thick filament. The high helical selectivity of the rigor myosin attachment provides an explanation of both the strong first row-line intensities on the 39-nm and 19-nm layer lines and the "ladder-like" stack of smooth outer layer lines (instead of the "helix cross" pattern expected from a uniformly labeled helix) in terms of Fourier components of the marking of the actin helix by cross-bridge mass (Fig. 2 *E*; Holmes et al., 1980).

There are two potential sources of the 38.7-nm layer line intensity in relaxed or stretch-activated IFM. One is the array of myosin heads on the thick filament, which is a four-start 152-nm helix (Wray, 1979; Morris et al., 1991; Reedy et al., 1993). The other is the two-start 77-nm helix of actin (Reedy, 1968; Miller and Tregear, 1972). Both would produce a layer line with 38–39-nm spacing, and in principle, both could contribute to the first row line (10.6 reflection) on the observed 38.7-nm layer line (hereafter referred to as the 39-nm layer line). However, the low equatorial radius of the first row line probably precludes a contribution to the 10.6 intensity from the myosin head array on the thick filament. For the thick filament array to diffract on the first row line, it would have to show strong helical order at a high radius about the thick filament, because the four-start helix generates a fourth-order Bessel function that peaks well out on the 39-nm layer line. Moreover, there is no sign of first row-line intensity on the 23-nm layer line of relaxed IFM, a state in which thick filament-based ordering predominates, and there is no first row-line intensity on the calculated 39-nm layer line from the thick filament model, whose computed diffraction most successfully matches the relaxed x-ray diagram (Hudson, 1997).

The other source of the first row line (10.6 reflection) on the 39-nm layer line is periodic marking of the actin helix. There are two possible candidates for such marking, the myosin head and the troponin. It was initially supposed that slight cross-bridge labeling in relaxed IFM caused the relaxed 10.6, for the high stiffness of relaxed IFM suggested significant weak binding of cross-bridges to actin (Pringle, 1967; White, 1983; Granzier and Wang, 1993), and the marked rise in 10.6 intensity upon fixation of relaxed IFM suggested the trapping of natural bridge contacts with actin targets (Reedy et al., 1983a,b). However, later work showed that a portion of the high-molecular-weight IFM troponin marks the actin helix with a bulge at each 39-nm-spaced half-turn (Bullard et al., 1988), and observations of AMP-PNP effects on rigor indicated that the troponin marking could explain independent changes in the two first row-line intensities (Reedy et al., 1987). If no myosin heads attach to actin in relaxed muscle, the troponin alone could produce the relatively strong first row-line reflection on the 39-nm layer line (10.6) and weak first row line reflection on the 19-nm layer line (10.12), because there would be only one marking of the actin long helix for each 39 nm (Fig. 5 *A*). As myosin attached in activation, its mass would add to that of the troponin in marking the actin helix. If these stretch-activated myosin heads attached preferentially to the same actins as the rigor lead bridges, whose target zone is midway between troponins (Reedy et al., 1994; Winkler et al., 1996; Schmitz et al., 1996), they would produce the observed effects: the first Fourier component of marking (the first row line of the 39-nm layer line) would be reduced because the troponin and myosin would destructively interfere, reducing the intensity of the 10.6, whereas for the second Fourier component (the first row line on the 19-nm layer line) they should constructively interact, thereby increasing the 10.12 (Fig. 5 *B*; see also Appendix 1). In this model, as the "lead bridge" target zone is progressively filled with cross-bridges, the 10.6 will first reduce, pass through zero, and then increase again, whereas the 10.12 will monotonically increase with increasing lead bridge occupancy. The two reflections should thus change in opposite directions at low lead bridge occupancy, as observed here.

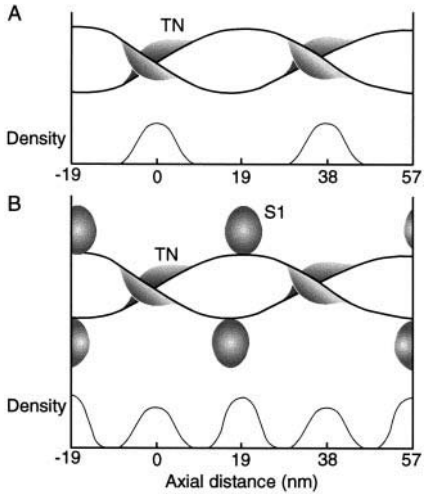

FIGURE 5 Proposed model for the opposed changes in intensity of the first row line peaks, 10.6 and 10.12, on the 38.7-nm and 19.3-nm layer lines. (*A*) Marking by troponin, as proposed for relaxed muscle. (*B*) Marking by troponin plus one (or less than one) S1 in the "lead bridge" target zone, as proposed for stretch-activated muscle. The axial distribution of density due to the suggested actin marking is shown below each cartoon. The localized marking densities do not necessarily represent the whole mass of troponin or S1, but only that portion of each that forms periodic ordered elements of extra mass along the thin filament.

TABLE 2 Relative intensities of reflections under differing conditions

	Intensity of reflection (as % of $I_{(20.0)}$ in relaxation) in			
		Calcium activation when		
Reflection	Relaxation	Unstretched	At peak tension	Rigor
10.6	1.52	1.38	0.76	4.22
11.6	0.34	0.27	0.41	1.96
20.6	0.37	0.45	0.55	0.69
21.6	0.26	0.28	0.42	1.88
30.6	0.19	0.19	0.01	0.44
22.6	0.21	0.24	0.20	0.48
31.6	0.17	0.26	0.43	1.72
10.12	0.10	0.12	0.37	1.45
00.16	56.97	53.41	25.50	2.40
00.32	3.69	3.20	2.40	0.24

The present data were compared between experimental conditions by relating them all to the 20.0 reflection in relaxation, on the assumption (Tregear et al, 1979; Rapp et al, 1991) that
$I(20.0)_{\text{calcium primed}} = 1.05\ I(20.0)_{\text{relaxation}}$,
$I(20.0)_{\text{stretch-activated}} = 1.10\ I(20.0)_{\text{relaxation}}$,
$I(20.0)_{\text{rigor}} = 1.50\ I(20.0)_{\text{relaxation}}$.

The rise in intensity of the outer reflections on the 39-nm layer line

The outer reflections on the 38.7-nm layer line are affected by the amount of mass following the actin helix. Therefore, their intensities are potential indicators of the number of cross-bridges attached to the actin helix during tension generation, if the contributions of myosin binding to the layer line can be separated from those of troponin, actin, and the array of heads on the thick filament. The 11.6 and 21.6 show increases that are not present in relaxed stretch (Fig. 3, *H* and *J*), whereas the 31.6 shows a rise that is partially duplicated in relaxed stretch (Fig. 3 *M*). The 20.6 rises (Fig. 3 *I*), but not significantly (Table 1), whereas the 30.6 and 22.6 both fall (Fig. 3, *K* and *L*). If the actin filaments take up a perfect $P6_4$ symmetry in the lattice, those contributors to the 39-nm layer line whose lattice indices are both even (20.6, 22.6) should destructively interfere, thereby weakening these reflections (Holmes et al., 1980). Indeed, the 20.6 and 22.6 reflections are weak in rigor, where $P6_4$ symmetry probably operates (Fig. 2 *E*; Table 2). The fall in the 30.6 reflection cannot be assigned to $P6_4$ symmetry, because it is not an even-even reflection, but it also decreases in relaxed stretch (Fig. 3 *K*). For these reasons, we have discounted the 20.6, 22.6, and 30.6 reflections, leaving the 11.6, 21.6, and 31.6 reflections as potential indices of the number of cross-bridges attached to the actin helix during stretch activation.

Another complication to interpreting the outer reflections in terms of the number of attached myosin heads is that not only does the myosin array on the thick filament generate the 14.5-nm meridional and the 23-nm layer line of relaxed muscle (Reedy, 1967), but modeling suggests that it also contributes to the outer part of the 39-nm layer line (Hudson, 1997). The 23-nm layer line reflects the degree of helical ordering of the myosin heads on the thick filament, and the 14.5-nm meridional reflects the ordering of the heads in the 14.5-nm collars. On calcium priming, the 23-nm layer line intensity almost disappears, and on stretch activation the 14.5-nm meridional intensity drops greatly, indicating that the ordering of the myosin heads on the thick filaments is much reduced. It is therefore probable that the contribution of the relaxed myosin head array on the thick filament to the outer portion of the 39-nm layer line also decreases during calcium priming and stretch activation. This would tend to reduce the apparent rise in intensity due to cross-bridge attachment to actin.

The fall in intensity of the 14.5- and 7.2-nm meridional reflections

The decreases in the meridional reflections on the 14.5-nm (00.16) and 7.2-nm (00.32) lines correlate closely with active tension. Previous diffraction observations in active IFM have shown that the 00.16 reflection decreases sharply as active tension rises, both in work-producing oscillation (Armitage et al., 1975) and after a sudden stretch (Rapp et al., 1991). The present data confirm this decrease. In addition, we show that the 7.2-nm meridional (00.32) decreases with a similar time course and that these changes do not reverse as rapidly as does active tension (Fig. 4 *A*). As with the 38.7-nm layer line, we must define the structure generating the diffraction to interpret these changes.

The arrays of myosin heads in vertebrate skeletal muscle and IFM thick filaments, and their reactions to activation, are quite different from each other. In relaxed vertebrate muscle, myosin heads are axially splayed, lie close to the

thick filament surface, and show a 14.3-nm/42.9-nm axial repeat. On activation there is a shift in spacing of the meridional from 14.3 to 14.5 nm that correlates with actin attachment. Actin-attached myosin heads contribute to this 14.5-nm reflection (Irving et al., 1992), which remains relatively high, even in rigor (Huxley and Brown, 1967). In contrast, the IFM thick filament is a four-start helix (Wray, 1979), from which the myosin heads project at right angles to the filament, forming axially distinct "shelves" of detached cross-bridges at 14.5-nm intervals (Menetret et al., 1990; Reedy et al., 1992, 1993). Such a structure has been shown by modeling to generate the strong 00.16 and 00.32 reflections, the weak 23-nm layer line, and the outer intensities of the 39-nm layer line (Hudson, 1997). On activation of IFM, there is no obvious change in the meridional spacing of the reflections, and the 14.5-nm intensity falls. In rigor IFM it virtually disappears, as do the 14.5-nm "shelves" on the thick filament (Reedy et al., 1965).

Decrease in 14.5-nm meridional intensity in active IFM could be caused by lateral broadening along the 14.5-nm layer line. Such lateral broadening is thought to indicate filament misregister. However, we find that only a small part of the 00.16 intensity spreads radially along the 14.5-nm layer line as tension rises, whereas Rapp et al. (1991) could see no broadening of the 00.16 peak on stretch activation. Therefore, filament misregister is unlikely to be a significant cause of 14.5-nm meridional intensity loss during stretch activation. A more likely cause of intensity loss on the 14.5-nm reflection is axial motion of individual myosin heads away from their confinement within the 14.5-nm shelves, due to either motion toward or attachment to actin. Whether actin-attached myosin heads contribute to the 14.5-nm meridional reflection of IFM, as they do in vertebrate skeletal muscle, remains to be determined; the near-absence of this reflection in rigor IFM indicates that they may not do so.

The equatorial intensities change little

The intensity changes on the equator are also different in IFM and vertebrate skeletal muscles. In vertebrate skeletal muscle the 11.0 reflection rises sharply slightly in advance of tension generation, as if there were a pronounced radial motion of the myosin heads (Kress et al., 1986; Harford and Squire, 1992). For actin attachment to occur, the axially splayed heads of relaxed vertebrate skeletal muscle would have to extend radially from the thick filaments. In contrast, in IFM the 20.0 reflection rises only slightly when priming calcium is added, and by a similar small amount in synchrony with the tension when IFM is stretch activated, either by oscillatory length changes (Miller and Tregear, 1970; Armitage et al., 1975) or by sudden step stretch (Rapp et al., 1991), as if there were only a small shift in radial cross-bridge position during tension generation. This is compatible with the already extended 90° myosin head position in Hudson's relaxed IFM model and the electron-microscopic appearance of the relaxed heads described above. The near-absence of equatorial change during stretch activation, in concert with the other signals of actin attachment, indicates that upon activation, the radial motion of myosin heads is only slight.

Quantitation of myosin attachment

To relate the intensity changes on tension generation to the number of myosin heads attached, we have adopted a model in which the active myosin heads are assumed to move from the thick filament array and attach to actin as they do in rigor. The model considers only the two extreme structures for the myosin head, either completely on the thick filament or completely on the thin filament, and ignores intermediates (for details see Appendix 1). The analysis uses the spatial modulation function developed by Holmes et al. (1980) and Yagi (1996), which defines the pattern of distribution of mass along thick filament and actin filament and thus allows one to interpret the intensity changes in terms of the emptying of a relaxed structure and the filling of a rigor structure. On this basis, the fall in the 14.5-nm meridional (00.16 reflection) on stretch activation suggests that at least 30% of the myosin heads leave the relaxed structure at the peak of tension, whereas the smaller fall in the 7.2-nm meridional (00.32 reflection) fits with only a 12% departure (Appendix, Δn_{tens}). These values are minima, because if attached myosin heads contributed to the meridional intensity (as they do in vertebrate skeletal muscle), more heads would have to move out of the relaxed array to produce the observed decreases. In future we hope to test whether they do so by observing the 00.16 reflection intensity during rapid length step perturbations of activated fibers (Lombardi et al., 1995).

The large fall in the 38.7-nm (10.6) reflection on stretch activation (Table 2) represents, in this model, an attachment of only 7% of the total available myosin heads, compared to the 75–80% that attach in rigor. It follows from the four-stranded nature of the insect thick filament that there are 3.56 myosin heads present in the muscle matrix per 38.7-nm half-turn on each side (or strand) of the actin helix, so 7% represents approximately one-quarter of a head per actin strand per half-turn during stretch activation (Appendix, Δp_{tens}). This small figure arises because of the reversal of sign in the amplitude of the 10.6 reflection; according to the model, as small numbers of heads bind to actin, the sign of the reflection passes through zero, which makes the 10.6 intensity highly sensitive to the initial cross-bridge binding at the lead bridge target zone. On the other hand, the similar rise in the 19-nm (10.12) reflection represents 23% of the available myosin heads, or 0.80 heads per actin strand per half-turn, because in the model this intensity is much less sensitive to initial cross-bridge binding. The outer reflections on the 38.7-nm layer line, 11.6, 21.6, and 31.6, as pointed out above, cannot be interpreted directly on the model. However, if one simply assumes that the number of

myosin heads attached is proportional to the square root of the observed intensity, and that 2.75 myosin heads attach to each actin strand per half-turn in rigor (Schmitz et al., 1996), these three reflections indicate that 0.38–0.45 myosin heads attach per actin strand per half-turn during stretch activation. It is not clear which of the above estimates is more reliable, but they all indicate that under the conditions of our experiments, a much smaller fraction of the available myosin heads forms a stereoselective attachment to the actin than the fraction that does so in rigor.

The conclusion that the fraction of myosin heads attached to actin is small is also consistent with the absence of density close to the meridian of the 5.9-nm layer line during tension generation (Fig. 2 *C*). An increase in intensity on the 5.9-nm line close to the meridian is expected to occur when myosin mass closely follows the 5.9-nm actin period, as when myosin binds in rigor (Fig. 2 *E*). Two factors may have contributed to the absence of change on this outer layer line in our experiments: the low fraction of myosin heads attached, as estimated from the results on the inner actin layer lines, and the more exact order required for the attached heads to diffract at the higher angle. This region of the diffraction pattern needs closer study.

CONCLUSIONS

In summary, it is probable that on stretch activation at least 30% of the myosin heads move out of the relaxed array, and that between 7% and 23% (or 0.25–0.8 per actin half-turn) attach to target zones similar to those in rigor. This represents on average less than one S1 head on each side of actin in each 39-nm helix half-turn, compared to nearly three per side in rigor. In view of the low amount of attachment and the reciprocal intensity changes in the 10.12 and 10.6 reflections, we propose that during stretch activation, active tension is generated principally by the action of single myosin heads at the lead bridge target zone. In three-dimensional reconstructions from electron micrographs of IFM fixed in a glycol-AMPPNP mixture, which produces a weakly bound static state (Tregear et al., 1990), the only ordered population of bridges consists of single heads attached at ~90° to the lead bridge target zones of actin (Schmitz et al., 1997). We have found that isometric activation of IFM by high calcium can give two to three times as much active tension as we have achieved by stretch activation (440 μN/fiber, compared to either 230 μN/fiber in stretch activation, or 140 μN/fiber if relaxed stretch tension is subtracted). Therefore, considerably greater myosin attachment than that seen in stretch activation probably occurs; whether this attachment is also helically selective and single-headed remains to be determined.

The present measurements support the proposition that in striated muscle more myosin heads are displaced from their relaxed position during tension generation than are attached to actin. The small increase in the intensity of the inner part of the 37-nm layer line found during isometric contraction of frog and rabbit skeletal muscle is believed to represent a minority of the myosin heads (Yagi, 1991; Harford and Squire, 1992; Bordas et al., 1993; Bershitsky et al., 1997); there is evidence that a greater number of cross-bridges are displaced toward actin during vertebrate striated muscle's contraction than make a precise actin contact (Kress et al., 1986; Martin-Fernandez et al., 1994).

The azimuthally favorable actin target zones marked so clearly by rigor cross-bridges in IFM are also recognized in rigor vertebrate skeletal muscle. In electron micrographs of rigor fish muscle, cross-bridge target zones can be seen and are related to the 36.5-nm period of the actin helix rather than the 39-nm period of troponin (Varriano-Marston et al., 1984); a target-zone model has also been shown to fit with the x-ray diffraction from rigor fish muscle (Squire and Harford, 1988). There is no clear evidence for actin helical orientation preference in electron micrographs from active vertebrate muscle (Tsukita and Yano, 1985; Hirose et al., 1993), but in single-molecule studies with the optical trap, S1 shows a preference for motion-generating attachment at each half-turn of the actin helix (Molloy et al., 1995). Thus the orientational selectivity that we suggest for IFM may be a general feature of thick and thin filament interaction, and hence of muscle function.

APPENDIX: MODEL OF SOURCES OF DIFFRACTION AT THE 00.16, 00.32, 10.12, 10.6, 11.6, 21.6, AND 31.6 REFLECTIONS

The purpose of this model is to provide a basis for quantitative interpretation of the changes in diffraction seen on these layer lines, in terms of movement of unattached myosin heads from their regular array on the thick filament and on to the actin helix. The model assumes that myosin heads are either on the relaxed thick filament array or, on disturbance or attachment, randomized relative to it. This assumption is based on the disappearance of both the 00.16 reflection and the electron-microscopic thick filament "shelves" when relaxed IFM is rigorized (Reedy et al., 1965), in contrast to the maintenance of a relatively strong 14.5-nm meridional in rigor vertebrate muscle (Huxley and Brown, 1967). The 00.16 and 00.32 reflections are considered to arise only from the thick filament head array, so the first two Fourier components of its axial distribution can be derived from them.

During attachment, the model supposes that the myosin heads attach in a uniform pattern, intercalating between troponins that are already positioned at a 38.7-nm spacing. Thus the attached myosin heads and troponin bulges form a composite of invariant pattern along the actin helix, although filling of the myosin sites changes. To avoid computation of transforms from unavailable detailed structural models, it is necessary to make the assumption that the form factors (but not the masses) of the attached myosin head and the projecting troponin component of IFM (Bullard et al., 1988) are similar at low resolution. The diffraction amplitudes from the two proteins can then be deduced from the intensities, provided that there is no other contributing mass. The first row-line reflections 10.6 and 10.12 arise only from the Fourier components of the actin helix labeling, as produced by the myosin and troponin, and not from its uniform labeling (Holmes et al., 1980), so this condition is fulfilled, allowing the first two Fourier components of the labeling pattern to be deduced from the intensities of the particular reflections. The condition is not fulfilled for the rest of the 39-nm layer line reflections, which are dependent on all of the contributing components, and on the filling of the array of unattached heads (Hudson, 1997).

In detail, the assumptions used are

1. The diffracting objects to be considered in accounting for the reflections 00.16, 00.32, 10.12, 10.6 are myosin heads and troponin.

2. In relaxation all myosin heads are arrayed on the thick filament at 14.5-nm intervals on a four-start 152-nm helix (Morris et al., 1991). Numerically this is equivalent to the presence of 3.56 myosin heads available to each side of a 39-nm length of actin filament.

3. In rigor 2.7–2.8 (75–80% of 3.56) myosin heads are bound to each side of the 39-nm pseudorepeat of the two-start actin helix, of which two are consistently at the lead bridge target zone and the third is usually in the rear bridge target zone (Schmitz et al., 1996).

4. Troponin is bound at each 39-nm half-turn of the thin filament, and a considerable portion of its mass is located at a specific region forming a bulge intermediate between the lead bridge target zones (Bullard et al., 1988; Schmitz et al., 1996).

5. In relaxation there are no myosin heads arrayed on the actin.

6. Myosin heads leave the relaxed thick filament array completely, and isotropically, i.e., once attached or disturbed by activation, a myosin head no longer contributes to this order, and all heads within the array are equally likely to be disturbed.

7. Myosin heads stereospecifically attach to actin in the same pattern of distribution in rigor or in active tension generation.

8. The form factor for the projecting troponin may be taken as similar to that for an attached myosin head at the resolution considered.

Consider the array of unattached myosin heads. Adopting the terminology of Holmes et al. (1980) for the diffraction from a nonuniformly filled array, the Fourier transform defining the diffraction from the myosin heads on the thick filament (F(thick)) is

$$F(\text{thick}) = L\{Q_{\text{th}}[M(\text{S1})]\}$$

where, working from the lowest level outwards, S1 is the form factor of the myosin head, M is the thick filament helix operator, Q_{th} is the spatial modulation function that describes the distribution of the myosin heads along the thick filament helix, and L is the lattice operator, placing the entire structure into the filament lattice. According to the present model, all except Q_{th} are constant. Q_{th} can be decomposed into Fourier components, $q(\text{th})_1$ for the fundamental, $q(\text{th})_2$ for the first harmonic, and so on. Each Fourier component gives rise to a diffraction pattern displaced meridionally from the origin by the spatial frequency. Hence the meridionals observed are measures of the strength of the Fourier components. For the thick filament the fundamental spatial frequency is 1/14.5 nm, so that for the 00.16 reflection, $Q_{\text{th}} = q(\text{th})_1$, and for the 00.32, $Q_{\text{th}} = q(\text{th})_2$. Furthermore, as the form of the array is assumed to remain constant under changing conditions, both components are proportional to the overall filling of the array. It follows that for the 00.16 and 00.32 reflections in a particular state i, the detached myosin head array gives an intensity

$$I_{\text{i}} = (n_{\text{i}}a_1)^2$$

where n_{i} is the number of myosin heads present in the thick filament array, and a_1 is the amplitude contribution for a myosin head. The number of heads detached from the thick filament array during tension generation ($\Delta n_{\text{tens}} = n_{\text{prestr}} - n_{\text{pktens}}$) is

$$\Delta n_{\text{tens}} = N(I^{1/2}_{\text{pre-str}} - I^{1/2}_{\text{pktens}})/I^{1/2}_{\text{rel}} \qquad (1)$$

where $N = 3.56$/side of an actin 39-nm pseudorepeat is the total number of heads available. Thus, on this model, the meridionals give two independent estimates of Δn_{tens}.

Now consider the thin filament array. The diffraction from the thin filament array (F(thin)) is

$$F(\text{thin}) = L\{Q_{\text{S1}}[A(\text{S1})] + Q_{\text{tn}}[A(\text{tn})] + Q_{\text{ac}}[A(\text{ac})]\}$$

where tn is the form factor of the troponin, ac is the form factor of the actin monomer, A is the actin helix operator, and Q_{S1}, Q_{tn} are the spatial modulation functions for S1 and troponin along the actin long helix. These can also be expressed as Fourier components. Actin fills the structure evenly, so that it has only a q_0 component. It follows that for reflections that arise solely from the operation of q_1 and q_2, respectively, the third term can be neglected. If we further assume that $A(\text{tn}) = A(\text{S1})$, the expression for such reflections (F'(thin)) simplifies to

$$F'(\text{thin}) = L\{(Q_{\text{S1}} + Q_{\text{tn}})[A(\text{S1})]\}$$

According to the present model, all of the factors in this equation except Q_{S1} are constant as conditions are varied. As with the previous case, the nonuniform filling of the structure gives rise to patterns meridionally offset from the origin by the spatial frequency of the distribution, in this case 1/39 nm. The meridionals of these displaced patterns are not present, because of the operation of the lattice (Holmes et al., 1980). However, the first row-line reflections (10.6, 10.12) can be used as measures of the strength of these displaced patterns; the first row-line is of too small an equatorial spacing to arise from the helical order of the decorated thin filament (Holmes et al., 1980). For the 10.6 reflection, $Q_{\text{S1}} = q(\text{S1})_1$, and for the 10.12, $Q_{\text{S1}} = q(\text{S1})_2$. Again, as the form of the array remains constant, both components are proportional to the overall filling of the array. The values of Q_{tn} for the two reflections are constants. It follows that for the 10.6 and 10.12 reflections in a particular state i, the attached myosin head array gives an intensity

$$I_{\text{i}} = [(p_{\text{i}} + \beta k)a_2]^2$$

where p_{i} is the number of myosin heads present in the attached myosin head array, a_2 is the amplitude contribution for a myosin head/troponin, k is the amount of troponin present (in myosin head units), and β is a function to phase it relative to the myosin head. If the myosin head and troponin attach to actin 19 nm apart, which is half the spatial frequency (Schmitz et al., 1996; Fig. 5), $\beta = \cos \pi = -1$ for the 10.6, and $\beta = \cos 2\pi = 1$ for the 10.12.

Consider first the 10.6 reflection. When the summed amplitude of the S1 and troponin remains the same sign as that of the troponin, the number of heads attached to the lead bridge array during tension generation ($\Delta p_{\text{tens}} = p_{\text{pktens}} - p_{\text{prestr}}$) is therefore

$$\Delta p_{\text{tens}} = P(I^{1/2}_{\text{pre-str}} - I^{1/2}_{\text{pktens}})/(I^{1/2}_{\text{rig}} + I^{1/2}_{\text{rel}}) \qquad (2a)$$

where P is the number of heads that attach in rigor; $P = 2.75$/side of an actin 39-nm pseudorepeat (Schmitz et al., 1996). The components of the denominator are added because the amplitudes in rigor and relaxation are of opposite sign.

When the sign of the summed amplitudes reverses during tension generation, the numerator also becomes an addition:

$$\Delta p_{\text{tens}} = P(I^{1/2}_{\text{pktens}} + I^{1/2}_{\text{pre-str}})/(I^{1/2}_{\text{rig}} + I^{1/2}_{\text{rel}}) \qquad (2b)$$

The 10.12 is a measure of the second Fourier component of mass distribution along the 39-nm pseudorepeat. The troponin and myosin head components are therefore in phase and of the same sign. It follows that this estimate of bridge attachment has the same algebraic form as Eq. 1. Thus for the 10.12,

$$\Delta p_{\text{tens}} = P(I^{1/2}_{\text{pktens}} - \text{I}^{1/2}_{\text{pre-str}})/(I^{1/2}_{\text{rig}} - I^{1/2}_{\text{rel}}) \qquad (3)$$

Thus these two reflections provide independent estimates of Δp_{tens}.

The numerical values of the parameters derived from Table 2, calculated as myosin heads/39 nm of one side of the actin helix, and giving in parentheses the percentage of the total number of heads available (3.56 per side per 39 nm), are as follows:

From the 00.16, $\Delta n_{\text{tens}} = 1.06$ (30%).
From the 00.32, $\Delta n_{\text{tens}} = 0.44$ (12%).
From the 10.6, $\Delta p_{\text{tens}} = 0.25$ (7%).
From the 10.12, $\Delta p_{\text{tens}} = 0.80$ (23%).

We thank Chris Bond for technical support with electronics. We thank SRS for providing visitors with on-site support and the Babraham Institute for

the loan of equipment. RTT thanks the MRC for laboratory, office, and computing facilities.

Purchase of the Güth muscle biophysics workstation used for x-ray diffraction of IFM was supported in part by a Muscular Dystrophy Association research grant and a National Institutes of Health Small Instrumentation grant. MKR, MCR, and RJE were also supported in part by National Institutes of Health grant AR-14317 to MKR. Travel to Daresbury Synchrotron by U.S. participants was supported in part by NATO Collaborative Research grant 900222.

REFERENCES

Armitage, P. M., R. T. Tregear, and A. Miller. 1975. Effect of activation by calcium on the x-ray diffraction pattern from insect flight muscle. *J. Mol. Biol.* 92:39–53.

Bershitsky, S. Y., A. K. Tsaturyan, O. N. Bershitskaya, G. I. Mashanov, P. Brown, R. Burns, and M. A. Ferenczi. 1997. Muscle force is generated by myosin heads stereospecifically attached to actin. *Nature.* 388: 186–190.

Bordas, J., G. P. Diakun, F. G. Diaz, J. E. Harries, R. A. Lewis, J. Lowy, G. R. Mant, M. L. Martin-Fernandez, and E. Towns-Andrews. 1993. Two-dimensional time-resolved X-ray diffraction studies of live isometrically contracting frog sartorius muscle. *J. Muscle Res. Cell Motil.* 14:311–324.

Brenner, B., and L. C. Yu. 1993. Structural changes in the actomyosin cross-bridges associated with force generation. *Proc. Natl. Acad. Sci. USA.* 90:5252–5256.

Bullard, B., K. Leonard, A. Larkins, G. Butcher, C. Karlik, and E. A. Fyrberg. 1988. Troponin of asynchronous flight muscle. *J. Mol. Biol.* 204:621–637.

Granzier, H. L. M., and K. Wang. 1993. Interplay between passive tension and strong and weak binding cross-bridges in insect indirect flight muscle. A functional dissection by gelsolin-mediated thin filament removal. *J. Gen. Physiol.* 101:235–270.

Güth, K., and R. Wojciechowski. 1986. Perfusion cuvette for the simultaneous measurement of mechanical, optical and energetic parameters of skinned muscle fibres. *Pflugers Arch.* 407:552–557.

Harford, J. J., and J. M. Squire. 1986. "Crystalline" myosin cross-bridge array in relaxed bony fish muscle. Low-angle x-ray diffraction from plaice fin muscle and its interpretation. *Biophys. J.* 50:145–155.

Harford, J. J., and J. M. Squire. 1992. Evidence for structurally different attached states of myosin cross-bridges on actin during contraction of fish muscle. *Biophys. J.* 63:387–396.

Hirose, K., C. Franzini-Armstrong, Y. E. Goldman, and J. M. Murray. 1994. Structural changes in muscle crossbridges accompanying force generation. *J. Cell Biol.* 127:763–778.

Hirose, K., T. D. Lenart, J. M. Murray, C. Franzini-Armstrong, and Y. E. Goldman. 1993. Flash and smash: rapid freezing of muscle fibers activated by photolysis of caged ATP. *Biophys. J.* 65:397–408.

Holmes, K. C., R. T. Tregear, and J. Barrington Leigh. 1980. Interpretation of the low angle x-ray diffraction from insect muscle in rigor. *Proc. R. Soc. Lond. (Biol.).* 207:13–33.

Hudson, L. 1997. Ultrastructure of the A band unit cell in relaxed muscle. Ph.D. dissertation. Imperial College, London University, London.

Huxley, H. E. 1969. The mechanism of muscular contraction. *Science.* 164:1356–1366.

Huxley, H. E., and W. Brown. 1967. The low-angle x-ray diagram of vertebrate striated muscle and its behaviour during contraction and rigor. *J. Mol. Biol.* 30:383–434.

Huxley, H. E., and M. Kress. 1985. Crossbridge behaviour during muscle contraction. *J. Muscle Res. Cell Motil.* 6:153–161.

Irving, M. 1993. Birefringence changes associated with isometric contraction and rapid shortening steps in frog skeletal muscle fibres. *J. Physiol. (Lond.).* 472:127–156.

Irving, M., V. Lombardi, G. Piazzesi, and M. A. Ferenczi. 1992. Myosin head movements are synchronous with the elementary force-generating process in muscle. *Nature.* 357:156–158.

Jewell, B., and J. Ruegg. 1966. Oscillatory contraction of insect fibrillar muscle after glycerol extraction. *Proc. R. Soc. Lond. (Biol.).* 164: 427–459.

Kress, M., H. E. Huxley, A. R. Faruqi, and J. Hendrix. 1986. Structural changes during activation of frog muscle studied by time-resolved X-ray diffraction. *J. Mol. Biol.* 188:325–342.

Lenart, T. D., J. M. Murray, C. Franzini-Armstrong, and Y. E. Goldman. 1996. Structure and periodicities of crossbridges in relaxation and during contraction initiated by photolysis of caged calcium. *Biophys. J.* 71: 2289–2306.

Levine, R. J. C. 1993. Evidence for overlapping myosin heads on relaxed thick filaments of fish, frog, and scallop striated muscles. *J. Struct. Biol.* 110:99–110.

Lombardi, V., G. Piazzesi, M. A. Ferenczi, H. Thirlwell, I. Dobbie, and M. Irving. 1995. Elastic distortion of myosin heads and repriming of the working stroke in muscle. *Nature.* 374:552–555.

Martin-Fernandez, M. L., J. Bordas, G. Diakun, J. Harries, J. Lowy, G. R. Mant, A. Svensson, and E. Towns-Andrews. 1994. Time-resolved x-ray diffraction studies of myosin head movements in live frog sartorius muscle during isometric and isotonic contractions. *J. Muscle Res. Cell Motil.* 15:319–348.

Menetret, J. F., R. R. Schröder, and W. Hofmann. 1990. Cryo-electron microscopic studies of relaxed striated muscle thick filaments. *J. Muscle Res. Cell Motil.* 11:1–11.

Miller, A., and R. T. Tregear. 1970. Evidence concerning crossbridge attachment during muscle contraction. *Nature.* 226:1060–1061.

Miller, A., and R. T. Tregear. 1972. The structure of insect fibrillar flight muscle in the presence and absence of ATP. *J. Mol. Biol.* 70:85–104.

Molloy, J. E., J. E. Burns, J. C. Sparrow, R. T. Tregear, J. Kendrick-Jones, and D. C. S. White. 1995. Single-molecule mechanics of heavy meromyosin and S1 interacting with rabbit or *Drosophila* actins using optical tweezers. *Biophys. J.* 68(Suppl.):298S–305S.

Morris, E. P., J. M. Squire, and G. W. Fuller. 1991. The 4-stranded helical arrangement of myosin heads on insect (*Lethocerus*) flight muscle thick filaments. *J. Struct. Biol.* 107:237–249.

Pringle, J. W. S. 1967. The contractile mechanism of insect fibrillar muscle. *Prog. Biophys. Mol. Biol.* 17:1–60.

Rapp, G., K. Güth, Y. Maéda, K. J. V. Poole, and R. S. Goody. 1991. Time-resolved x-ray diffraction studies on stretch activated insect flight muscle. *J. Muscle Res. Cell Motil.* 12:208–215.

Rayment, I., H. M. Holden, M. Whittaker, C. B. Yohn, M. Lorenz, K. C. Holmes, and R. A. Milligan. 1993. Structure of the actin-myosin complex and its implications for muscle contraction. *Science.* 261:58–65.

Reedy, M. K. 1967. Cross-bridges and periods in insect flight muscle. *Am. Zool.* 7:465–481.

Reedy, M. K. 1968. Ultrastructure of insect flight muscle. I. Screw sense and structuural grouping in the cross-bridge lattice. *J. Mol. Biol.* 31: 155–166.

Reedy, M. K., R. S. Goody, W. Hofmann, and G. Rosenbaum. 1983a. Coordinated electron microscopy and X-ray studies of glycerinated insect flight muscle. I. X-ray diffraction monitoring during preparation for electron microscopy of muscle fibers fixed in rigor, in ATP and in AMPPNP. *J. Muscle Res. Cell Motil.* 4:25–53.

Reedy, M. K., K. C. Holmes, and R. T. Tregear. 1965. Induced changes in orientation of the cross-bridges of glycerinated insect flight muscle. *Nature.* 207:1276–1280.

Reedy, M. K., C. Lucaveche, N. Nariber, and R. Cooke. 1992. Insect crossbridges, relaxed by spin-labeled nucleotide, show well-ordered 90° state by x-ray diffraction and electron microscopy, but spectra of electron paramagnetic resonance probes report disorder. *J. Mol. Biol.* 227: 678–697.

Reedy, M. K., C. Lucaveche, M. C. Reedy, and B. Somasundaram. 1993. Experiments on crossbridge action and filament sliding in insect flight muscle. *Adv. Exp. Med. Biol.* 332:33–44.

Reedy, M. K., and M. C. Reedy. 1985. Rigor crossbridge structure in tilted single filament layers and flared-X formations from insect flight muscle. *J. Mol. Biol.* 185:145–176.

Reedy, M. C., M. K. Reedy, and R. S. Goody. 1983b. Coordinated electron microscopy and x-ray studies of glycerinated insect flight muscle. II. Electron microscopy and image reconstruction of muscle fibers fixed in rigor, in ATP and in AMPPNP. *J. Muscle Res. Cell Motil.* 4:55–81.

Reedy, M. C., M. K. Reedy, and R. S. Goody. 1987. The structure of insect flight muscle in the presence of AMPPNP. *J. Muscle Res. Cell Motil.* 8:473–503.

Reedy, M. C., M. K. Reedy, K. R. Leonard, and B. Bullard. 1994. Gold/Fab immuno-electron-microscopy localization of troponin H and troponin T in *Lethocerus* flight muscle. *J. Mol. Biol.* 239:52–67.

Reedy, M. C., M. K. Reedy, and R. T. Tregear. 1988. Two attached non-rigor crossbridge forms in insect flight muscle. *J. Mol. Biol.* 204: 357–383.

Schmitz, H., M. C. Reedy, M. K. Reedy, R. T. Tregear, and K. A. Taylor. 1997. Tomographic three-dimensional reconstruction of insect flight muscle partially relaxed by AMPPNP and ethylene glycol. *J. Cell Biol.* 139:695–707.

Schmitz, H., M. C. Reedy, M. K. Reedy, R. T. Tregear, H. Winkler, and K. A. Taylor. 1996. Electron tomography of insect flight muscle in rigor and AMPPNP at 23°C. *J. Mol. Biol.* 264:279–301.

Squire, J. M., and J. J. Harford. 1988. Actin filament organization and myosin head labelling patterns in vertebrate skeletal muscles in the rigor and weak binding states. *J. Muscle Res. Cell Motil.* 9:344–358.

Taylor, K. A., M. C. Reedy, L. Córdova, and M. K. Reedy. 1989a. Three-dimensional image reconstruction of insect flight muscle. II. The rigor actin layer. *J. Cell Biol.* 109:1103–1123.

Taylor, K. A., M. C. Reedy, L. Córdova, and M. K. Reedy. 1989b. Three-dimensional image reconstruction of insect flight muscle. I. The rigor myac layer. *J. Cell Biol.* 109:1085–1102.

Taylor, K. A., M. C. Reedy, M. K. Reedy, and R. A. Crowther. 1993. Crossbridges in the complete unit cell of rigor insect flight muscle imaged by three-dimensional reconstruction from oblique sections. *J. Mol. Biol.* 233:86–108.

Tregear, R. T., K. Wakabayashi, H. Tanaka, H. Iwamoto, M. C. Reedy, M. K. Reedy, H. Sugi, and Y. Amemiya. 1990. X-ray diffraction and electron microscopy from *Lethocerus* flight muscle partially relaxed by adenylylimidodiphosphate and ethylene glycol. *J. Mol. Biol.* 214: 129–141.

Tsukita, S., and M. Yano. 1985. Actomyosin structure in contracting muscle detected by rapid freezing. *Nature.* 317:182–184.

Varriano-Marston, E., C. Franzini-Armstrong, and J. C. Haselgrove. 1984. The structure and disposition of crossbridges in deep-etched fish muscle. *J. Muscle Res. Cell Motil.* 5:363–386.

Wakabayashi, K., H. Tanaka, H. Saito, N. Moriwaki, Y. Ueno, and Y. Amemiya. 1991. Dynamic X-ray diffraction of skeletal muscle contraction: structural change of actin filaments. *Adv. Biophys.* 27:3–13.

White, D. C. 1983. The elasticity of relaxed insect fibrillar flight muscle. *J. Physiol. (Lond.).* 343:31–57.

White, D. C. S., M. M. K. Donaldson, G. E. Pearce, and M. G. A. Wilson. 1977. The resting elasticity of insect fibrillar muscle and properties of the crossbridge cycle. *In* Insect Flight Muscle: Proceedings of the Oxford Symposium. R. T. Tregear, editor. Elsevier, Amsterdam. 197–208.

White, D. C. S., and J. Thorson. 1972. Phosphate starvation and the nonlinear dynamics of insect fibrillar flight muscle. *J. Gen. Physiol.* 60:307–336.

Winkler, H., M. C. Reedy, M. K. Reedy, R. T. Tregear, and K. A. Taylor. 1996. 3-D structure of nucleotide-bearing crossbridges in situ: oblique section reconstruction of insect flight muscle in AMPPNP at 23°C. *J. Mol. Biol.* 264:302–322.

Wray, J. S. 1979. Filament geometry and the activation of insect flight muscles. *Nature.* 280:325–326.

Yagi, N. 1991. Intensification of the first actin layer-line during contraction of frog skeletal muscle. *Adv. Biophys.* 27:35–43.

Yagi, N. 1996. Labelling of thin filaments by myosin heads in contracting and rigor vertebrate skeletal muscles. *Acta Crystallogr.* D52: 1169–1173.